Equivalent circuit analysis of terahertz metamaterial filters

(Invited Paper)

Xueqian Zhang (张学迁)[1], Quan Li (李 泉)[1], Wei Cao (曹 伟)[2], Weisheng Yue (岳伟生)[3], Jianqiang Gu (谷建强)[2], Zhen Tian (田 震)[2], Jiaguang Han (韩家广)[1*], and Weili Zhang (张伟力)[1,2]

[1] *Center for Terahertz Waves and College of Precision Instrument and Optoelectronics Engineering, and Key Laboratory of Opto-electronics Information Technology, Ministry of Education, Tianjin University, Tianjin 300072, China*

[2] *School of Electrical and Computer Engineering, Oklahoma State University, Stillwater, Oklahoma 74078, USA*

[3] *Advanced Nanofabrication, Imaging and Characterization Core Facilities, King Abdullah University of Science and Technology, Thuwal 23955, Saudi Arabia*

[*] *Corresponding author: jiaghan@tju.edu.cn*

Received July 1, 2011; accepted August 8, 2011; posted online September 30, 2011

An equivalent circuit model for the analysis and design of terahertz (THz) metamaterial filters is presented. The proposed model, derived based on LMC equivalent circuits, takes into account the detailed geometrical parameters and the presence of a dielectric substrate with the existing analytic expressions for self-inductance, mutual inductance, and capacitance. The model is in good agreement with the experimental measurements and full-wave simulations. Exploiting the circuit model has made it possible to predict accurately the resonance frequency of the proposed structures and thus, quick and accurate process of designing THz device from artificial metamaterials is offered.

OCIS codes: 160.3918, 300.6495.
doi: 10.3788/COL201109.110012.

Metamaterials have been demonstrated over a significant portion of the electromagnetic spectra from radio, microwave, and terahertz (THz) to the optical regimes. The unique properties of metamaterials are not attainable with naturally occurring materials[1]. Thus, enormous applications in devices and techniques, such as superlens, cloaking, antenna, and sub-wavelength photolithography are enabled[2−5]. The capability of metamaterials has been broadly expanded because they allow precise control of the electromagnetic responses. The appreciation of electromagnetic response control through metamaterial structures provides unique benefits in the design of versatile devices, including filters, modulators, and switchable components.

However, geometry strongly influences the electromagnetic performance of metamaterials. Consequently, it is necessary to formulate some models that can accurately predict their behaviors have been formulated. Several models have been put forward, such as the LC resonant model[6], TL-RLC model[7], Fano model[8], and dipole resonance model[9]. In most of previous investigations, however, the models are limited because it is difficult to provide a specific value for each circuit parameter needed to fabricate a given component. This is particularly true for a complex design. In this letter, an equivalent circuit model is proposed. The model combines an LMC resonator with the existing analytic expressions for the capacitive and inductive elements. The analytical model agrees well with the experimental measurements and the full-wave simulations for various designs.

Because of their wide applications in sensing, spectroscopy, imaging, security, and so forth, filters have become one of the most important devices. Based on the most commonly used U-shaped resonators[10,11], a metamaterial filter design is chosen, i.e., a merged double-U (MDU) split ring resonator (SRR) structure with normal incident electromagnetic field orientations, as shown in Fig. 1. The proposed structure offers relevant opportunities and considerable flexibilities to control the electromagnetic response over a broad THz frequency range.

Two exactly consistent U-shape resonators are merged oppositely to form a "MDU molecule." The inset of Fig. 1 shows the diagram of a unit cell of MDU, where the U-shape resonators have fixed geometric parameters: U leg length $l = 45$ μm, lateral width $d = 40$ μm, and line width $w = 5$ μm, but with various overlapping distances between the two Us. The overlapping distances

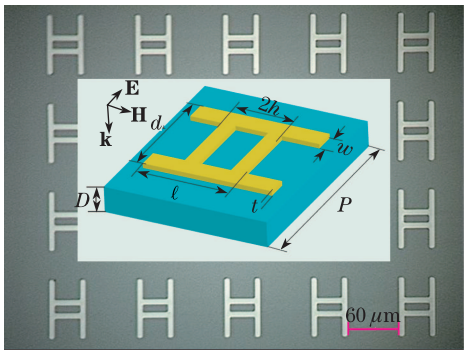

Fig. 1. Microscopic image of the MDU array. Inset: typical structure of MDU with a definition of the geometrical parameters.

between the two Us are quantified by the length h, where $h = 0$ occurs when the fused Us begin to separate. The MDU resonators with 200-nm-thick Al metal structures on a square lattice of period $P = 100$ μm are fabricated on a 640-μm-thick silicon substrate by conventional photolithography processing. This is shown in Fig. 1. To characterize experimentally the properties of the MDU resonators, an 8-F THz time-domain spectroscopy (TDS) transmission system is employed[12]. By arranging the parabolic mirrors in a confocal geometry, the excellent beam is focused to a frequency-independent beam waist. The beam waist is approximately 3.5 mm at the center between the transmitter and the receiver where we locate the reference and the sample. The respective transmission spectra $E_{\rm in}(\omega)$ and $E_{\rm out}(\omega)$ of the reference and sample are both experimentally characterized. The reference is a blank Si slab identical to the sample's substrate. The amplitude transmission $t(\omega) = |E_{\rm out}(\omega)/E_{\rm in}(\omega)|$ is subsequently calculated with respect to ω, the angular frequency.

Figure 2(a) presents the microscopic images of the measured structures for the different values of overlap distance $h \in [7, 19]$ μm. The measured values $t(\omega)$, $\omega/2\pi \in [0.4, 1.3]$ THz, reveal a sharp dip in the amplitude transmission, indicating the characteristic of a band-stop filter. The resonance dip blueshifts gradually from 0.59 to 0.87 THz as h is increased from 7 to 19 μm, as shown in Fig. 2(b). The transmission dip remains $\sim$0.15 during this increase in h, with Q-factors of 7.70 for $h = 7$ μm and 6.81 for $h = 19$ μm.

The measured spectral response characteristics of the chosen structures are further supported by a full wave numerical simulation using CST Microwave Studio. The unit cell shown in Fig. 1 is used in the simulations under periodic boundary conditions. The silicon substrate is modeled as a lossless dielectric material with relative permittivity of $\varepsilon_{\rm Si} = 11.78$, while Al is simulated with a conductivity of $\sigma_{\rm Al} = 3.72 \times 10^7$ S/m. The simulated spectra of $t(\omega)$ in Fig. 2(c) reveal good agreement with the experimental data in Fig. 2(b).

Figure 3 illustrates the simulated distributions of the electric field and surface current density in the unit cell for different values of h at the corresponding resonance frequencies. The electric field is concentrated around the ends of the four legs in each case (shown in the second line). The surface current density (shown in the first line), (i) is symmetric in relation to the axis parallel to and equidistant from the two cross-bars, (ii) is antisymmetric in relation to the central axis normal to

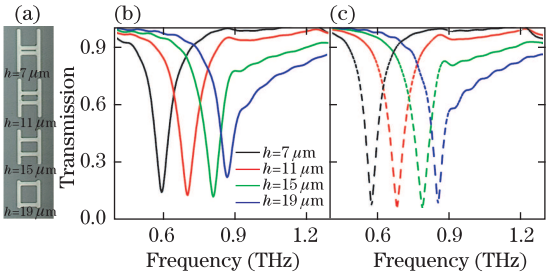

Fig. 2. (a) Microscopic images of measured structures with different h; (b) measured values of the transmission amplitude for four different values of h; (c) simulated spectra of the transmission amplitude of the band-stop filter.

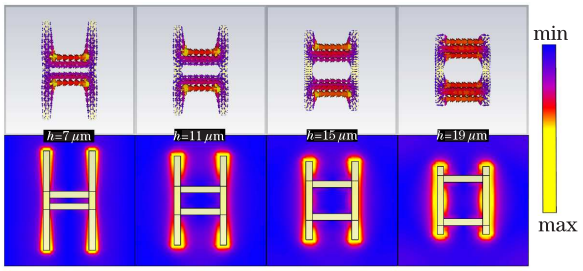

Fig. 3. (a) Simulated surface current (first line) and electric field distribution (second line) of the structures with different values of h at resonant frequencies. The arrows indicate the induced surface current direction, and the color represents the electric field density.

the cross-bars, and (iii) is concentrated along the two cross-bars. Accordingly, if an equivalent-circuit model for the merged-U structure should be formulated, each bar must have self-inductance, and some bar pairs must have mutual inductance. However, any inductances for the central bars that are between and orthogonal to the two cross-bars can be ignored because of antisymmetry.

Based on the analysis above, an equivalent LMC circuit model is established for the unit cell. This is shown in Fig. 4(a). L_1 is the self-inductance of each leg, and L_2 is the self-inductance of each cross-bar. M_1 and C_1 are the mutual inductance and capacitance between the oppositely facing legs, respectively. M_2 is the mutual inductance between the two cross-bars, and C_2 is the capacitance between the central bars that are orthogonal to the cross-bars.

To apply the LMC circuit model, it is necessary to calculate all equivalent circuit parameters. Using the line capacitance theory[13], we obtain

$$C_1 = a_1\varepsilon_0\varepsilon_{\rm eff}(\ell - 2h)\frac{K(k_0')}{K(k_0)}, \tag{1}$$

$$C_2 = a_2\varepsilon_0\varepsilon_{\rm eff}(h - w)\frac{K(k_0')}{K(k_0)}, \tag{2}$$

where a_1 and a_2 are the unknown coefficients; $K(k_0)$ is the complete elliptic integral of the first kind with $k_0 = d/(d+2w)$ and $k_0' = \sqrt{1-k_0^2}$; ε_0 is the permittivity of free space, and $\varepsilon_{\rm eff} = f\varepsilon_{\rm Si} + (1-f)$ is the effective relative permittivity that accounts for the contributions of both air and the substrate to the capacitance, where $f \in (0, 1)$ is a factor representing the effect of the substrate. The members of the set $\{a_1, a_2, f\}$ can be fixed by fitting them against the three experimental data sets.

The self-inductance of each current-carrying surface is calculated according to the Bueno theory[14]:

$$\Lambda(\ell_0) = \frac{\mu_0\ell_0}{4\pi}\Big[2\sinh^{-1}\Big(\frac{\ell_0}{w}\Big) + (1+n)\Big(\frac{\ell_0}{w}\Big)\sinh^{-1}\Big(\frac{w}{\ell_0}\Big) - \frac{(3-n)}{3}\frac{(w^2+\ell_0^2)^{3/2}}{\ell_0 w^2} + (1-n)\frac{\ell_0}{w^2}(w^2+\ell_0^2)^{1/2} + \frac{2n}{3}\Big(\frac{\ell_0}{w}\Big)^2 + \frac{3-n}{3}\Big(\frac{w}{\ell_0}\Big)\Big], \tag{3}$$

where ℓ_0 is the length of the bar, μ_0 is the permeability of free space, and n is an integer number. In Eq. (3), the Neumann model is used with $n = 1$. Thus, Eq. (3) is simplified to:

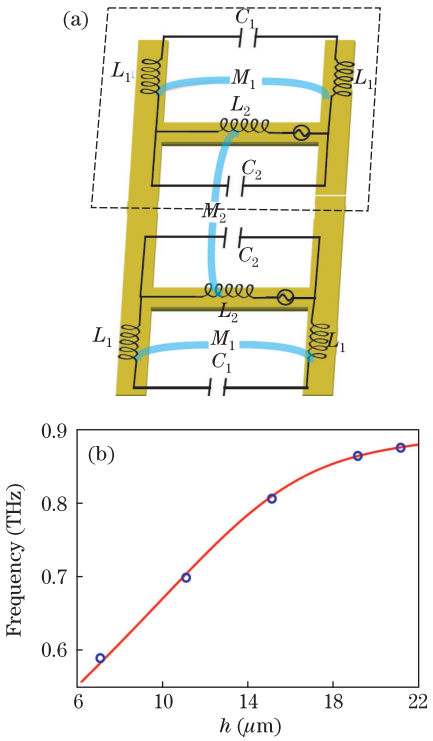

Fig. 4. (Color online) (a) Equivalent-circuit model of the MDU structure. The blue lines between the parallel bars represent mutual inductances. The half of the structure surrounded by the red dashed line is the part we consider for the production of equivalent circuit. (b) Measured (open circles) and fitted frequency (solid curve) of the LMC circuit model as functions of h.

$$\Lambda(\ell_0) = \frac{\mu_0 \ell_0}{4\pi}\left\{2\sinh^{-1}\left(\frac{\ell_0}{w}\right) + 2\left(\frac{\ell_0}{w}\right)\sinh^{-1}\left(\frac{w}{\ell_0}\right) + \frac{2}{3}\left[\left(\frac{\ell_0}{w}\right)^2 + \frac{\ell_0}{w} - \frac{\left(w^2+\ell_0^2\right)^{3/2}}{\ell_0 w^2}\right]\right\}. \quad (4)$$

Specifically, the self-inductances in our structures can be calculated as: $L_1 = \Lambda(\ell - 2h)$ and $L_2 = \Lambda(d)$. In addition, the mutual inductance between the two parallel bars of length ℓ_0, separated by distance h_0, and with current densities pointed in the same direction can be expressed as[14]

$$\Xi\left(\ell_0, h_0\right) = \frac{\mu_0}{4\pi}\left\{2\ell_0 \sinh^{-1}\left(\frac{\ell_0}{h_0}\right) + 2\left[h_0 - \left(h_0^2+\ell_0^2\right)^{1/2}\right]\right\}. \quad (5)$$

For our unit cell, $M_1 = -\Xi(l - 2h, d - w)$ and $M_2 = \Xi(d, 2h - w)$. The negative sign in M_1 is a result of the opposite direction of the surface current density. Thus, the total impedance of the half circuit is given as

$$Z_{\rm m} = \left[\frac{1}{{\rm j}\omega C_1} + {\rm j}\omega(2L_1 + 2M_1)\right] // \frac{1}{{\rm j}\omega C_2} + {\rm j}\omega(L_2 + M_2). \quad (6)$$

The resonance frequency can be extracted through the relation:

$$\mathrm{Im}(Z_{\rm m}) = 0. \quad (7)$$

Figure 4(b) presents a detailed LMC circuit model fitted on the resonance frequency for $h \in [6, 22]$ μm. The solid line in Fig. 4(b) represents the analytically predicted resonance frequency by the LMC model with $\{a_1 = 0.057, a_2 = 0.107, f = 0.54\}$, which is in good agreement with the experimental results. The calculations indicate that the increase of h results in the decrease of C_1, L_1, and M_2 as well as the increase of C_2 and M_1. However, L_2 is independent of h (Table 1). Therefore, the presented MDU structure provides a good choice for terahertz bandstop filters, and the complementary design of the MDU structure can serve as a good terahertz bandpass filter according to the Babinet's principle[15].

To verify the effectiveness of the LMC circuit model, we changed the other parameters of the MDU structure with fixed h. Figure 5(a) shows the microscopic images of the measured structures with fixed values, i.e., $h = 42$ μm and $d = 40$ μm but with various values of U leg length $\ell \in [27, 51]$ μm. The measured and simulated transmission spectra are shown in Figs. 5(b) and (c), respectively. The resonance frequency redshifts gradually from 0.889 to 0.607 THz as l is increased from 27 to 45 μm with an interval of 8 μm. Using the identical LMC circuit model previously shown, we obtain the agreeable fitting curve (Fig. 5(d)) with $\{a_1 = 0.044, a_2 = 0.258, f = 0.54\}$, which is also in good agreement with the experimental results. Table 2 provides the circuit parameters for the different values of l.

In addition, we fixed the values, i.e., $h = 42$ μm and $l = 40$ μm, but made the value of d variable (Fig. 6(a)). Figures 6(b) and (c) present a remarkable redshift of amplitude transmission with dip enhancement, as d changes from 30 to 90 μm. Compared with the MDU structure shown in Fig. 1, the structure in this case has its own characteristics: (i) from the point of view of the simulated electric field distribution and surface current, the mutual inductance effect between the two cross-bars in a unit cell is smaller than the effect between the two adjacent cross-bars in the two neighboring unit cells,

Table 1. Obtained Circuit Parameters in the LMC Model for Various Values of h ($l = 45$ μm, $d = 30$ μm, and $w = 5$ μm)

h (μm)	7	11	15	19	21
L_1 (pH)	19.036	12.883	7.1948	2.4457	0.6801
L_2 (pH)	26.509	26.509	26.509	26.509	26.509
M_1 (pH)	–2.5980	–1.4630	–0.6335	–0.1395	–0.0257
M_2 (pH)	11.178	7.4370	5.5579	4.4186	4.0028
C_1 (fF)	1.0088	0.7485	0.4881	0.2278	0.0976
C_2 (fF)	0.1222	0.3665	0.6109	0.8552	0.9774

Table 2. Obtained Circuit Parameters in the LMC Model for Various Values of l ($d = 30$ μm, $w = 5$ μm, and $h = 10$ μm)

l (μm)	27	35	43	51
L_1 (pH)	2.4457	7.1948	12.833	19.036
L_2 (pH)	26.509	26.509	26.509	26.509
M_1 (pH)	–0.1395	–0.6335	–1.4630	–2.5980
M_2 (pH)	8.1153	8.1153	8.1153	8.1153
C_1 (fF)	0.1758	0.3768	0.5778	0.7787
C_2 (fF)	0.7365	0.7365	0.7365	0.7365

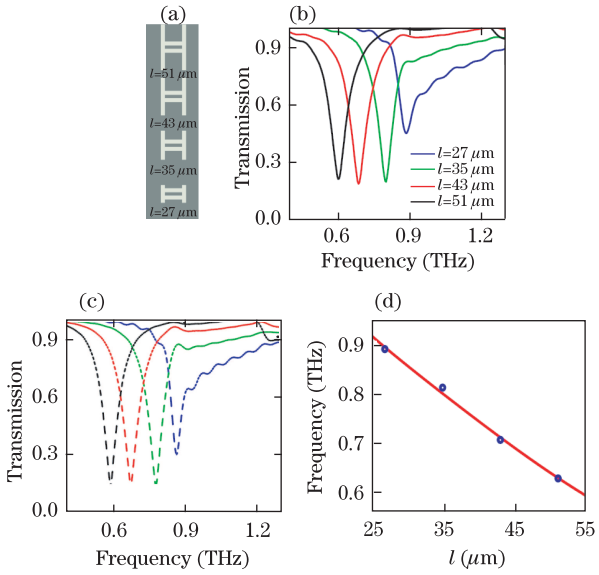

Fig. 5. (a) Microscopic images of measured structures with different l; (b) measured values of the transmission amplitude for four different values of l; (c) simulated amplitude transmission as a function of l; (d) measured (open circles) and fitted frequency (solid curve) of the LMC circuit model as functions of l.

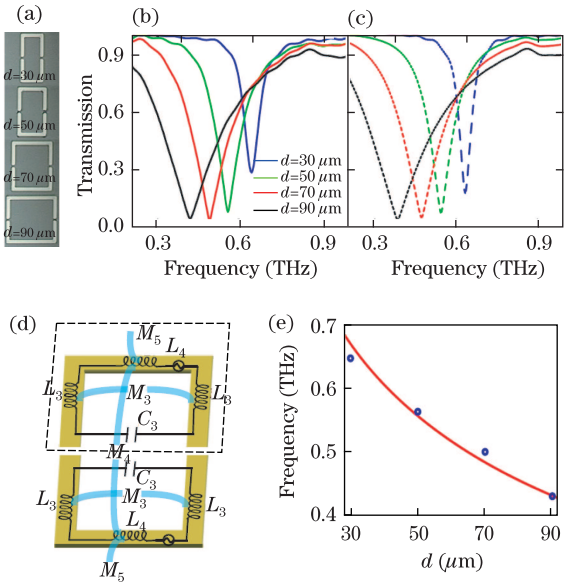

Fig. 6. (a) Microscopic images of the measured structures with different d; (b) measured amplitude transmission as a function of d; (c) simulated amplitude transmission as a function of d; (d) sketch of LMC circuit model for MDU structure of changing values of d; (e) measured (open circles) and fitted frequency (solid curve) of the LMC circuit model as functions of d.

leading to an extra mutual inductance M_5 (Fig. 6(d)); (ii) self-inductance and mutual inductance should be taken into consideration due to the gaps in the middle of the bars normal to the cross-bars. The LMC circuit model for this case is shown in Fig. 6(d). Although the LMC circuit model shows a slight difference compared with the previous one, all circuit parameters can still be calculated with the aforementioned equations. The

Table 3. Obtained Circuit Parameters in the LMC Model for Various Values of d ($l = 40$ μm, $w = 5$ μm, and $h = 42$ μm)

d (μm)	30	50	70	90
L_3 (pH)	22.301	22.301	22.301	22.301
L_4 (pH)	18.236	35.286	53.981	73.834
M_3 (pH)	–4.3635	–2.6048	–1.8426	–1.4218
M_4 (pH)	1.1261	3.0697	5.8686	9.4260
M_5 (pH)	3.8029	9.3747	16.448	24.628
C_3 (fF)	1.2748	1.0399	0.9322	0.8667

corresponding capacitances and inductances are depicted as: $C_3 = a_3\varepsilon_0\varepsilon_{\text{eff}}(l-w)\frac{K(k_0')}{K(k_0)}$, $L_3 = \Lambda(\ell - w)$, $L_4 = \Lambda(d)$, $M_3 = \Xi(l-w, d-w)$, $M_4 = \Xi(l, 2h-w)$, and $M_5 = \Xi(l, P-2h+w)$.

By solving Eq. (7), the expression of the resonance frequency can be obtained as:

$$f_0 = \frac{1}{2\pi\sqrt{(2L_3 + L_4 + 2M_3 + M_4 + M_5)C_3}}. \quad (8)$$

The red solid line in Fig. 6(e) represents the analytically predicted resonance frequency based on Eq. (8) with the following parameters: $\{a_3 = 0.113, f = 0.54\}$. The resonance is also in good agreement with the simulated results and enables us to confirm the validity of the LMC circuit model. The obtained circuit parameters are displayed in Table 3.

In conclusion, an equivalent LMC circuit model is presented. The capability for accurate analysis of the design of THz filters comprising a square array of subwavelength U-shape resonators is demonstrated as well. The model allows the derivation of an analytical expression of each circuit parameter and takes into account the presence of a dielectric substrate. Thus, the model can predict the resonance frequency of the proposed structures with very good accuracy. The results have been compared with both experimental measurements and full-wave simulations for various designs. Good agreement has been achieved, which indicates promising applications in terahertz device designs.

This work was supported by the National Natural Science Fondation of China (Nos. 61028011, 61007034, and 60977064), the U.S. National Science Foundation, the Tianjin Sci-Tech Program (Nos. 09ZCKFGX01500 and 10JCYBJC01400), and the 111 Program of China (No. B07014).

References

1. V. G. Veselago, Sov. Phys. Usp. **10,** 509 (1968).
2. J. B. Pendry, Phys. Rev. Lett. **85,** 3966 (2000).
3. R. Liu, C. Ji, J. J. Mock, J. Y. Chin, T. J. Cui, and D. R. Smith, Science **323,** 366 (2009).
4. R. W. Ziolkowski and A. Erentok, IEEE Trans. Antenn. Propag. **54,** 2113 (2006).
5. T. Xu, Y. Zhao, J. Ma, C. Wang, J. Cui, C. Du, and X. Luo, Opt. Express **16,** 13579 (2008).
6. V. Delgado, O. Sydoruk, E. Tatartschuk, R. Marqués, M. J. Freire, and L. Jelinek, Metamaterials **3,** 57 (2009).

7. S. Li, H. Zhang, Q. Wen, Y. Xie, D. Tian, and Y. Li, Appl. Phys. A **100,** 461 (2010).
8. X. Lu, J. Han, and W. Zhang, Appl. Phys. Lett. **92,** 121103 (2008).
9. X. Lu and W. Zhang, Appl. Phys. Lett. **94,** 181106 (2009).
10. C. Rockstuhl, F. Lederer, C. Etrich, T. Zentgraf, J. Kuhl, and H. Giessen, Opt. Express **14,** 8827 (2006).
11. I. M. Pryce, K. Aydin, Y. A. Kelaita, R. M. Briggs, and H. A. Atwater, Nano Lett. **10,** 4222 (2006).
12. D. Grischkowsky, S. Keiding, M. van Exter, and Ch. Fattinger, J. Opt. Soc. Am. B **7,** 2006 (1990).
13. S. Gevorgian and H. Berg, in *Proceedings of Microwave Conference 2001* (2001).
14. M. A. Bueno and A. K. T. Assist, J. Phys. D: Appl. Phys. **28,** 1802 (1995).
15. C. Rockstuhl, T. Zentgraf, T. P. Meyrath, H. Giessen, and F. Lederer, Opt. Express **16,** 2080 (2008).